IEEE Access
Multidisciplinary ⋮ Rapid Review ⋮ Open Access Journal

Received 31 May 2023, accepted 12 June 2023, date of publication 19 June 2023, date of current version 23 June 2023.

Digital Object Identifier 10.1109/ACCESS.2023.3287492

RESEARCH ARTICLE

An Antenna Solution for Glacial Environmental Sensor Networks

MUHAMMAD ABDUR REHMAN HASHMI[1,2], (Graduate Student Member, IEEE), AND PAUL V. BRENNAN[1]

[1]Department of Electronic and Electrical Engineering, University College London, WC1E 7JE London, U.K.
[2]Department of Electronics and Power Engineering, Pakistan Navy Engineering College (PNEC), National University of Sciences and Technology (NUST), Karachi 75350, Pakistan

Corresponding author: Muhammad Abdur Rehman Hashmi (Muhammad.hashmi.18@ucl.ac.uk)

ABSTRACT Antennas used in glacial environmental sensor networks and reported in the last two decades have been reviewed. A link budget framework for designing such antenna systems is presented and used to design an antenna system for deployment at the Thwaites glacier, Antarctica. Design details of two left hand circularly polarized cross dipole antennas, one for englacial sensor probes and the other for supraglacial surface receivers are presented. The probe antenna is a 3D bent cross dipole that fits within a borehole of 8 cm diameter while providing a 1 dBic gain at 433 MHz in ice. The surface receiver antenna is a planar printed antenna providing a gain of 6.1 dBic with a quarter wave reflector. Both antennas provide 3 dB beamwidths of at least 50° in the xz and yz vertical planes catering for transmitter-receiver antenna misalignments caused by extended deployments. The antennas displayed good circular polarization and polarization purity traits. The 3 dB axial ratio bandwidths of both the antennas remained 54.9 %. The total efficiencies of the bent cross dipole and the surface receiver antennas were noted as 69.7 % and 86.9 % respectively. Lastly, the 433 MHz band has been validated for achieving englacial communication ranges of up to 2300 metres.

INDEX TERMS Englacial sensor probe, link budget framework, cross dipole, glacier monitoring, bent cross dipole, planar printed antenna, 433 MHz frequency, communication through ice, Thwaites project.

I. INTRODUCTION

Glaciers, ice shelves, and ice sheets [1], [2] play an important role in our planet's ecosystem. The adverse consequences of melting ice masses could include changes in Earth's rotation and gravitational field [3], uncertainty in water supply [4], rise in sea levels [5], [6], [7], [8], floods [9], and climate change [10]. In recent years, the scientific community has made some efforts to measure different glaciological parameters and processes to predict glacier behaviour. Most in-situ monitoring techniques involve deploying sensor probes through boreholes, glacier crevasses, or portals. The sensor probes measure parameters like temperature, pressure, strain, and electrical conductivity, etc. Wireless probes are usually preferred over wired ones for multi-hundred metres deep deployments due to factors like basal sliding, potential cable breaks, and logistical issues, etc. A wireless sensor probe needs an antenna to transmit sensor data to a surface receiver (RX). At the surface, another antenna receives the transmitted sensor data. This paper makes the following contributions. Firstly, a review of antenna systems used in different glacial environmental sensor networks (ESNs) has been provided. The term 'antenna systems' includes the antenna used with sensor probe transmitter (TX) and the one used with surface RX. Secondly, a link budget framework to calculate antenna gain requirements of a glacial ESN is presented. Next, the framework has been used to calculate antenna gain requirements for the Thwaites project. This project is a collaboration between University College London (UCL) and the British Antarctic Survey (BAS). The Thwaites project aims to deploy numerous wireless englacial sensor probes at the Thwaites glacier, Antarctica to periodically measure parameters of shear strain, temperature, pressure, and tilt at different glacial layers. The sensor data will be

The associate editor coordinating the review of this manuscript and approving it for publication was Barbara Masini.

recorded over period of a year and subsequently analysed to learn about the trends in different glacier parameters. The sensor probes will be deployed at multiple sites through up to 2300 meters deep boreholes having a maximum usable diameter of 8 cm. The borehole diameter restricts the maximum diameter of the sensor probe accordingly. The third contribution of this paper is the design and development of two antennas tuned to 433 MHz for the Thwaites project. The first antenna is a 3D bent cross dipole made for englacial sensor probes. The second one is a planar printed cross dipole antenna for use with glacier surface RXs. None of the previous works used these antenna types for the said applications. The previous works used helical, coil ferrite, and dielectric resonator antennas (DRAs) for englacial sensor probes. Types of antennas previously used with surface RXs included Yagi, helical, non-printed cross dipole, and log periodic dipole array. Lastly, the feasibility of 433 MHz frequency has been investigated for multi-hundred metres communication through ice. Previous works used lower frequencies like 30 MHz, and 151 MHz to achieve such ranges.

The rest of the paper is organized as follows. Section II presents a review of antenna systems used in glacial ESNs reported in the last two decades and compares them with the proposed method and antennas. Feasibility of some non-planar/ quasi-planar antennas for glacial ESNs has also been discussed. Section III presents the proposed link budget framework to calculate antenna parameters. Section IV presents the 3D bent cross dipole and the planar printed cross dipole antenna designs. Section V discusses the simulated and measured results of the two antennas in ice/snow, and free space media. Finally, section VI concludes the paper.

II. RELATED WORKS

There are three major projects that deployed wireless glacial ESNs. The first one is the GlacsWeb project [11] and its subsequent works [12], [13], [14], [15], [16], [17], [18] that have been reported between 2003 and 2019. The second one is the Wireless sensor (WiSe) system [19] and its subsequent work [20] reported between 2010 and 2014. The third one is the Electronic tracer (E-tracer) project [21] and its subsequent works [22], [23] reported between 2009 and 2018. Besides these major projects, a few one-off related projects [24], [25] are also discussed. Table 1 provides a comparative review of the works that have used a 433 MHz wireless link. Table 2 presents a review on the same basis for works using sub-433 MHz frequencies.

A. GLACSWEB PROJECT AND ITS SUBSEQUENT WORKS

The GlacsWeb glacial ESN [11] used englacial probes with omni-directional DRAs [26], [27] tuned to 433 MHz for transmitting information to a surface base station. It is opined that an omni-directional DRA proved sufficient because of a short 50 to 80 metres communication distance. On the contrary, antennas in the Thwaites project need to communicate over almost 28 times larger distance. This necessitates the use of a directional antenna. One advantage of an omni-directional antenna in this application may be unrestricting the orientation of the sensor probe to affect communication performance. However, since both GlacsWeb and Thwaites projects use boreholes to deploy cylindrical sensor probes, the probes are expected not to lose their vertical orientation more than 25° probably even over a period of a year. Therefore, a directional antenna with a 3 dB beamwidth of 50° in both the vertical planes xz and yz should cater for the transmit-receive antenna misalignments caused by glaciological processes like basal sliding, etc. over a period of a year.

TABLE 1. A comparative review of works using 433 MHz frequency.

Work Ref.	Max range (m)	Sensor probe antenna type	Surface RX antenna type
This paper	2300	3D bent cross dipole	Planar printed cross dipole
[11]	80	Omni-directional dielectric resonator antenna (DRA)	Not published
[12]	72	Helical	Helical
[13]	70	Omni-directional DRA	Not published
[16]	69	--"--	--"--
[17]	86	--"--	--"--

In [12], helical antennas [28], [29], [30], [31] operating at 433 MHz were used both for the englacial probes and the surface RX. Helical antennas can generally provide better directivity as compared to an omni-directional DRA like the one used in [11]. The transmit distance through ice remained similar, with the probes deployed at depths between 19 to 72 meters. Primarily due to a shorter communication distance, a relatively larger link budget was available in [12] reducing the gain requirements for the antennas compared to the Thwaites project. The authors at [12] used the same helical antenna for both the probe and the surface RX when there were size restrictions probably only for the probe. However, different antennas are designed for probes and surface RXs in the Thwaites project. Since there is no size restriction for the surface antenna, just a portability requirement, an antenna with a relatively higher gain as compared to the probe antenna is used. In [13], K. C. Rose et al. used the GlacsWeb equipment [11] to successfully collect data from subglacial probes deployed at depths of 60-70 m. A DRA antenna operating at 433 MHz was used in the wireless subglacial probes.

K. Martinez et al. developed a wireless sensor network (WSN) [14] derived from the equipment initially developed for the GlacsWeb project [11]. The probes were deployed at depths of 60-80 m. The WSN [14] probes used a quarter wave helical antenna made from 24 s.w.g. wire and tuned at 173 MHz. Lower frequencies can generally provide longer ranges at the cost of larger antenna sizes. Since the probes in [14] were deployed only up to 80 m, probably an operating frequency of 433 MHz instead of 173 MHz would have also sufficed. In another deployment of this WSN [15], measurements with wireless probes were acquired with probes deployed at depths of up to 80 m. DRAs were used in probes deployed up to 69 m and 86 m in [16] and [17] respectively.

TABLE 2. A Comparative Review of Works using sub-433 MHz Frequencies.

Work reference	Maximum range	Communication link type and frequency	Sensor probe antenna type	Surface receiver antenna type
This paper	2300m	Wireless, 433 MHz	3D bent cross dipole	Planar printed cross dipole
[14]	80m	Wireless (173.25 MHz) and wired backup link	Quarter wave helical	Not published
[15]	80m	Wireless, 173.25 MHz	--"--	--"--
[18]	30m	Wired (RS-485 link) and wireless (173 MHz) backup link	Not published	Not published
[19]	2500m	Wireless, 30 MHz and Wired	Coil ferrite	(1) Non-printed cross dipole (2) Log periodic dipole array
[20]	320m	Wireless, 30 MHz	--"--	--"--
[21]	--	Wireless transmission for detection only, 151 MHz	Helical	Yagi
[22]	2000m	Wireless, 151 MHz	--"--	--"--
[23]	150m	Wireless, 151.6 MHz	--"--	--"--
[24]	Total: 502.5m; Wired: 500m; Wireless: 2.5m	Wired and wireless (450/510 Hz)	Coil around a core generates a magnetic field	Coil around a core senses changes in its magnetic field

In [18], four wired geophones were deployed at the base of a 30 m deep glacier to monitor seismic activities. The geophones' data was conveyed through a wired link to the surface nodes. There is a mention of a backup 173 MHz radio link which was probably not installed in the deployed geophones since when three out of the four geophones failed to communicate after a day's deployment, there is no mention of re-establishing communication through any backup radio link. Englacial environment is harsh and probably not suitable for long term deployment of wired probes. Failure of 75% of the deployed probes due to failed wired links with cables stretching to just 30 metres, perhaps confirms the aforesaid statement. A wireless link for subglacial probes is therefore probably a better option. The antennas operating at 433 MHz developed for the Thwaites project might be suitable candidates to provide a wireless link for a future deployment of the geophone probes to relatively higher depths.

B. WIRELESS SENSOR SYSTEM AND ITS SUBSEQUENT WORKS

Smeets et al. [19] have designed a wireless sensor system (WiSe) that is perhaps able to provide the antenna performance required for the Thwaites project as well. A coil ferrite antenna tuned to 30 MHz was used in the wireless probes [19], whereas a novel 3D bent cross dipole operating at 433 MHz has been developed for the Thwaites project. Two different types of RX antennas were used in [19] namely a non-printed cross dipole antenna and a HB9CV log periodic dipole antenna array. Successful communication was achieved when probes tied to a rope were lowered down to 2500 m deep boreholes. The HB9CV antenna performed better with a higher signal to noise ratio of the received signal compared to the cross-dipole antenna. The usage of ropes and a short time measurement probably helped with maintaining the vertical orientation of the probes and facilitated the probe antennas with keeping their main lobes in the upwards direction. For a more comprehensive test, the probes should have been left at the maximum depth for some extended period like 6 months or a year. Extended deployment would have made the probes undergo orientation changes due to the lateral movement of ice layers. This way the antennas could have been tested for suitable radiation patterns and adequate 3 dB beamwidths. The surface antennas developed in [19] were quite large since they were tuned to 30 MHz. This made them less portable and difficult to carry to remote sites with poor accessibility. On the other hand, the Thwaites project has aimed to develop robust and portable designs for the surface antennas and selection of 433 MHz transmit-receive frequency facilitates the use of relatively smaller sized receive antennas. In another work [20], the WiSe system [19] was used to achieve englacial communication ranges of up to 320 metres.

C. ELECTRONIC TRACER PROJECT AND ITS SUBSEQUENT WORKS

E-tracers [21] were spherical probes that measured water pressure along flow path of water channels in glaciers. E-tracers did not transmit the recorded data to a RX but stored it in some onboard memory. A TX operating at 151 MHz with a helical antenna was built into an E-tracer to facilitate its detection by a RX with a Yagi antenna once it emerged from a glacier portal. Contrary to E-tracers [21], sensor probes in Thwaites project need to wirelessly transmit the recorded data to a surface RX through up to 2300 m deep ice. The

antenna in an E-tracer was probably only required to transmit up to tens of metres to get detected by the tracking RXs. This reduces the performance requirements for both the TX and RX antennas. Probably a common desired feature for the RX antennas in [21] and the Thwaites project is their portability. The Moulin explorer [25] was another probe having similarities in its geometry and function with the E-tracer [21]. Two improved spherical probes called new E-tracer and Cryoegg were reported in [22] for the same application. These new probes used same antenna type and operating frequency as E-tracers [21] but they transmitted sensor data wirelessly while travelling. The Thwaites project aims to deploy probes in relatively static locations and capsule shaped probes are more suited than spherical ones as used in [22]. Capsule shaped probes are expected to maintain their vertical orientations better. Ranges of up to 2000 metres were achieved in [22]. The following are few reasons why the new E-tracers and Cryoeggs might not be suitable for the Thwaites project. Firstly, good ranges of up to 2000 m were achieved in [22] by using high power TXs with transmit powers of 100-500 mW. Such high power demands high battery power and therefore these TXs might not be a good candidate if the probes are to be left in the ice body for a long duration like a year, as required for the Thwaites project. Secondly, the probes in [22] use a lower frequency of 151 MHz since they are required to transmit reliably through wet glacial environment. Whereas the probes in the Thwaites project are expected to mostly encounter dry ice and therefore use 433 MHz. Thirdly, the Thwaites project requires probes not to be larger than 8 cm in diameter and house multiple sensors as well. While new E-tracers have 5 cm diameters, their spherical shape lets them house only one sensor, the Cryoeggs on the other hand are too big (12 cm diameter) to be used for the Thwaites project. Fourthly, E-tracers and Cryoeggs probably used omni-directional antennas since they are spherical in shape rendering them unable to maintain a particular orientation. The Thwaites project requires ranges of even better than 2000 m and therefore it makes sense to use directional antennas and capsule shaped casings to facilitate them maintain correct orientation in the ice body.

A 3D helical antenna tuned to 151.6 MHz was used in sensor probes called ET+ [23] to transmit information through 150 m of glacier body mostly firn, received at the surface with a Yagi antenna. Though the lower spectrum of the UHF band 300 MHz – 3 GHz may be satisfactory for transmission through dry ice, firn offers more attenuation due to a different internal structure and presence of melt water. Accordingly, the authors of [23] made use of a lower frequency 151.6 MHz as compared to the Thwaites project which uses 433 MHz, to mitigate effects of the additional attenuation offered by firn and snow as compared to dry ice.

D. BLACK RAPIDS PROJECT

In [24], a sensor probe installed 2.5 m deep in a glacier till wirelessly sent information to another probe near the ice-till interface. The later probe was connected to a surface RX through a wired link. For wireless communication, a coil wound around a core produced low frequency chirps of 450 Hz and 510 Hz to convey messages to a RX again consisting of a coil around a core but with a pre-amplifier. Probably, one of the reasons for using ultra low frequency (ULF) 300-3000 Hz for wireless communication here is the high electromagnetic (EM) signal attenuation caused by the glacier till composition to signals in relatively higher frequency bands. The antennas developed for the Thwaites project, may be of utility in such a project [24] by replacing the wired link between ice-till interface TX and the surface RX with a wireless one. Such a wireless link could provide higher communication ranges.

E. NON-PLANAR/QUASI-PLANAR ANTENNAS

Some non-planar/ quasi planar circularly polarized (CP) antennas [32], [33], [34], [35], [36], [37], [38], [39] were reviewed to gauge their feasibility for glacial ESN applications. Most of these antennas have been tested for relatively higher frequency bands like Ku [32], 10 GHz [35], 9.75 GHz [34], 5-6 GHz [39], 5.8 GHz [38], 5.2 GHz [33], 2.3 – 3.4 GHz [36], and 0.915/2.45 GHz [37]. They offer some desired features like low profile [32], [36], [37], [38], low axial ratio [33], [35], [36], realized gains of > 5 dBic [32], [34], [35], [38], [39], HPBWs of $> 50°$ [32], [33], and high radiation efficiency [37]. However, all these antennas have been tested at frequencies higher than 433 MHz, in free space medium only, and for applications other than glacial ESNs. Ice/ snow medium testing of scaled versions of these antennas tuned to frequencies like 173 MHz, 433 MHz, etc. might reveal interesting results and their feasibility for glacial ESNs could then be assessed.

The works reviewed either used a helical, coil ferrite or dielectric resonator antenna for the wireless sensor probes. Antennas used with surface RXs included Yagi, helical, non-printed cross dipole, and log periodic dipole array. Feasibility of recently reported non-planar/quasi-planar antennas [32], [33], [34], [35], [36], [37], [38], [39] for glacial ESN applications hasn't yet been assessed. Printed spiral and cross dipole antennas for surface RXs including [40], [41], [42] and the one presented in this paper for the Thwaites project haven't been assessed by previous projects. A comparative review of the proposed surface receiver antenna with [40], [41], [42] on the basis of 3 dB axial ratio percentage bandwidth (ARBW), realized gain, and total efficiency is provided in Table 3. For achieving ranges above 100 m, previously frequencies lower than 433 MHz were used.

III. A LINK BUDGET FRAMEWORK FOR ANTENNA SYSTEMS

For free space, the parameters that define the link budget of a communication system include TX power P_T, RX sensitivity P_R (the achievable data rate depends on it), free space wavelength λ, distance between the TX and RX antennas d, and finally the TX and the RX antenna realized gains

TABLE 3. A comparative review of antennas for glacial ESN applications.

Work Ref.	3 dB ARBW (%)	Realized gain at 433 MHz (dBic)	Total efficiency at 433 MHz (%)	Difference between co and cross polarization within a beamwidth of 60^0 at 433 MHz (dB)
Printed cross dipole antenna	54.9	6.1	86.9	10.1
[40]	54.9	5.9	88.7	11.6
[41]	54.9	7.4	96.3	7.7
[42]	100	6.7	97.7	7.7

denoted by G_{Tx} and G_{Rx} respectively. The Friis transmission equation [43] must be satisfied.

For reliable communication in snow/ice medium, some additional factors need to be considered. The EM wavelength changes in mediums with different dielectric constants. The effective wavelength λ_e can be found by $\lambda_e = \frac{\lambda}{\sqrt{\varepsilon_r}}$ where ε_r is the dielectric constant of the medium. Mediums like a glacier body don't offer a consistent dielectric constant throughout due to several reasons. Different glacier layers have different molecular compositions. For example, the top layer of snow is usually soft with an ε_r of 2.5 [44] followed by a layer of firn. The snow and firn layers usually extend up to a depth of 70 m, below which there is usually hard and thick ice with an ε_r of 3.1 [44]. Then, there are water channels in glaciers which offer a relatively higher attenuation to microwaves. The presence of acids, debris, and other materials like stones, rocks, etc. also affect EM wave propagation. These losses vary from site to site and one attenuation model probably can't be applied to two different sites. A generalized EM wave attenuation model is currently not available, though site-focused studies have been reported. For EM wave travel through a glacier, energy is primarily lost through geometric spreading commonly referred to as path loss P_L [45] and dielectric attenuation L [45], [46]. The dielectric attenuation depends upon the following factors: (1) temperature profile of glacier layers, (2) density, and (3) impurities which mainly include the acid contents. Other factors that affect EM wave propagation include birefringence and crystal orientation fabrics B [47], hydrostatic pressure, and finally air bubble shape. The two factors, namely hydrostatic pressure and air bubble shape have relatively negligible effects and could be ignored. Spatial variation in dielectric attenuation is mainly caused by changes in conductivity. The prime factor controlling conductivity is acidic impurity. Due to strong dependence on acidic contents, the dielectric attenuation L is almost frequency independent starting from a few megahertz up to several hundred megahertz. Acidity levels within Antarctic ice sheets are controlled by biogenic activity [45], volcanic activity, and periodic changes in precipitation ionic concentrations [46]. Effects of birefringence would become more pronounced with linearly polarized (LP) antennas than CP antennas. For example, if the ice crystal polarization is vertical and an LP antenna is horizontally polarized, the ice crystals would offer more resistance to EM waves. On the other hand, a CP antenna would generate circularly polarized waves, which would be relatively less attenuated by linearly polarized ice crystals of any orientation. Therefore, for a telemetry system operating in ice medium, the Friis equation [43] could be re-written in decibel units as shown in (1):

$$G_{Tx} + G_{Rx} = P_R - P_T - P_L + L - B \tag{1}$$

where $P_L = 20\log_{10}\left(\frac{\lambda_e}{4\pi d}\right)$. The influence of B is relatively less compared to P_L and L, and there are only 12% and 3% probabilities that it varies by more than 5 dB and 10 dB respectively [46]. Therefore, ignoring B, (1) can be re-written as (2):

$$G_{Tx} + G_{Rx} = P_R - P_T - P_L + L \tag{2}$$

Equation (2) holds true provided both the TX and RX antennas have the same polarization. In case of a polarization mismatch, a polarization loss factor (PLF) needs to be included in (2). If both TX and RX antennas are LP, PLF (in dB) is defined by (3) [48] where φ represents angle (in degrees) the TX antenna is rotated from the RX antenna:

$$\text{PLF} = 10\log_{10}\cos^2\varphi \tag{3}$$

A perfect alignment between the TX and RX antennas will give $\varphi = 0^0$ and PLF = 0 dB. If $\varphi = 90^0$ which would happen if, for example, the TX antenna is horizontally polarized and the RX antenna is vertically polarized, PLF $= -\infty$ and there would be no reception. If one antenna is CP and the other is LP, only 50% of the transmitted EM waves would be received, and PLF $= -3$ dB. If both antennas are left hand CP (LHCP) or right hand CP (RHCP), there would be no polarization loss and PLF = 0 dB. Considering PLF, (2) can be rewritten as (4):

$$G_{Tx} + G_{Rx} = P_R - P_T - P_L + L - \text{PLF} \tag{4}$$

The work at [47] provides some estimated values of L for different sites at the Antarctic ice sheet and the correct value should be chosen. Typical values of L range between 0.01 to 0.02 dB/m, with a maximum reported variation of 0 to 0.04 dB/m across the complete Antarctic ice sheet. For the Thwaites glacier experiment site chosen by BAS, L has been estimated as 0.02 dB/m, which represents a near worst case scenario and is a good estimate for most of the Antarctic sites usually used for radar and telemetry measurements. For the Thwaites project in particular, (4) could be re-written as (5):

$$G_{Tx} + G_{Rx} = P_R - P_T - P_L + 0.02d - \text{PLF} \tag{5}$$

where d is the distance between TX and RX antennas in metres. While (5) is suited to calculate link budgets for antennas at the Thwaites glacier site and most others in Antarctica, (4) provides a more generalized link budget framework. While [47], [49] provide estimates of L for Antarctica,

a recent work [50] has reported some values of L for Greenland.

As an example, we start by calculating the combined link budget of the TX and RX antennas for the Thwaites project. We set the parameters wavelength $\lambda_e = \frac{c_{lf}}{\sqrt{\varepsilon_r}} = 0.39$ m, c = speed of light $= 3 \times 10^8$ m/s, f = frequency = 433 MHz, and ε_r = ice dielectric constant = 3.1 [44], TX power P_t = 20 dBm and RX sensitivity P_R = - 121 dBm allowing a data rate of 4688 bps with the HopeRF RFM96W transceiver module, and a transmit distance d of 2300 m. Both the probe and surface antennas are assumed to be circularly polarized with the same sense and there is no loss due to a polarization mismatch. Therefore PLF = 0 dB. This gives $G_{Tx} + G_{Rx}$= 2.4 dB. Assuming RX antenna gain G_{Rx} of 5 dBic, the requirement for the TX antenna gain G_{Tx} comes out to be -2.6 dBic. Allowing an extra link margin of 2.6 dB to cater for unpredicted losses, a G_{Tx} of 0 dBic or above is very acceptable.

IV. ANTENNA DESIGNS

The Thwaites project imposed some design constraints on the antennas. A summary of these design considerations is provided next followed by the design details of two CP antennas: one to be used with the englacial sensor probe TX and the other with the glacier surface RX.

A. DESIGN CONSIDERATIONS

The TX antenna must fit inside a probe with an internal diameter of 8 cm due to limitations on the size of boreholes. The probe antenna also needs to conform to the probe assembly shape and facilitate installation of other electronics and batteries as well. Sensor probes will be left in the glacier for about a year. After a year of basal sliding, the antennas in englacial probes and surface RXs will undergo spatial lateral shifting and will no longer be aligned. It is estimated that a 3 dB beamwidth (in both xz and yz planes) of at least 50° for both the probe and surface antennas would be satisfactory. It is desirable to have simple, easily reproducible, and portable designs of antennas.

B. FEED NETWORK DESIGN OF CP CROSSED DIPOLE ANTENNAS

CP antennas made for both the TX and RX are novel variants of the crossed dipole design [51]. A crossed dipole antenna has four branches, and each branch is usually perpendicular to the adjacent ones. The branches are fed with phases of 0°, 90°, 180°, and 270° moving clockwise (CW) or counterclockwise (CCW). A CW feed sequence would produce RHCP antennas while a CCW feed order produces LHCP antennas. Both TX and RX antennas are designed as LHCP. To produce this quadrifilar feed with varying phases, a feed network was designed. A schematic diagram of the feed network is shown in Fig. 1(a), while its circuit diagram is shown in Fig. 1(b). The feed network is designed using one 180° and two 90° hybrid ICs on a double sided 0.8 mm FR-4 board

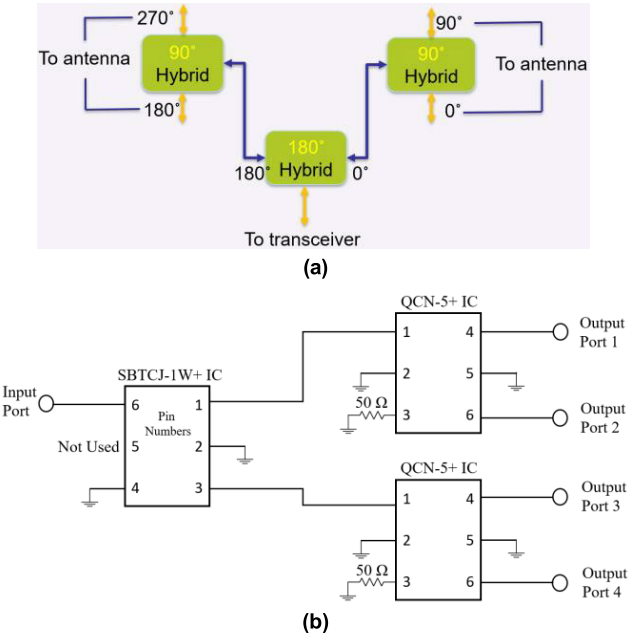

FIGURE 1. Feed network to generate a quadrifilar output, (a) Schematic diagram, (b) Circuit diagram.

($\varepsilon_r = 4.3, tan\delta = 0.025$). When working in the forward direction, a 180° hybrid IC splits up the signal from the transceiver equally into two parts having a phase difference of 180° between the two components. In the reverse direction, it combines two signals having a 180° phase shift into one. The 90° hybrid IC works similarly except that the phase shift is 90° instead of 180°. Mini-Circuits® ICs QCN-5+ and SBTCJ-1W+ have been selected as the 90° and 180° hybrid ICs respectively. The selected ICs support operation between 330-580 MHz and come in small packaging. Fig. 2 shows the geometric parameters of the feed network, whose values are listed in Table 4. The circularly shaped developed feed network with 4 × test SMA connectors is shown in Fig. 3. A circular PCB design offers two advantages. Firstly, it ensures minimal PCB size and a small ground plane. Any radiation going through the ground plane is lost and a small sized ground plane is thus desirable. Secondly, it facilitates maintaining symmetry of the traces to achieve good amplitude and phase balance. The feed network is fed at the bottom layer with a SSMA connector which has a smaller footprint than a SMA and helps keep the ground plane to a minimal size. Microstrip line width at 433 MHz 50 Ω was calculated using Keysight advanced design system (ADS) software and manually as well. Reverse manual calculations were done using [52] to validate the line width calculated by ADS.

It was desirable to achieve good amplitude and phase balance between the four ports. A good amplitude balance means minimal difference in amplitude across the 0°, 90°, 180°, and 270° phase outputs. A good phase balance refers to a phase difference as near as possible to 90° between any two adjacent ports. The quality of amplitude and phase balance influences the quality of circular polarization (CP) of the antenna. A good quality of CP helps the antenna in

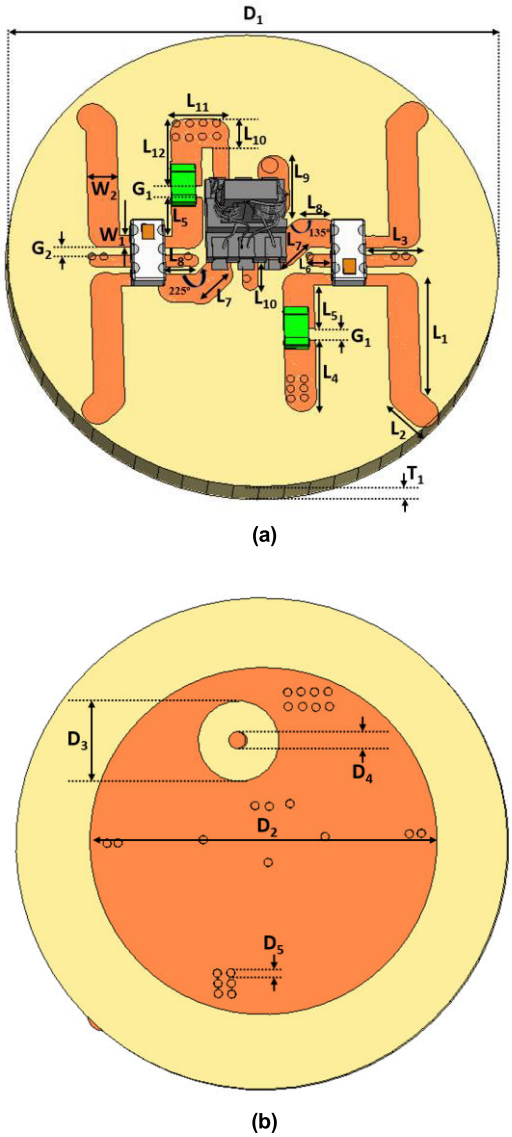

(a)

(b)

FIGURE 2. Antenna feed network, (a) Top layer, (b) Bottom layer.

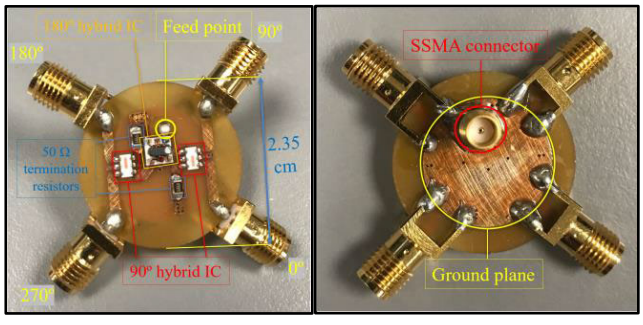

(a) (b)

FIGURE 3. Labelled pictures of the developed feed network, (a) Top layer, (b) Bottom layer.

maintaining a symmetric far field in both the xz and yz planes and a low axial ratio across the operating frequency range. Next, the two antenna designs are presented. Both the antennas make use of the same feed network.

TABLE 4. Geometric parameters of the feed network.

Parameter	Value (mm)	Parameter	Value (mm)
L_1	6.11	L_{12}	3.59
L_2	2.25	G_1	0.6
L_3	2.2	G_2	0.39
L_4	3.71	W_1	0.61
L_5	2.21	W_2	1.48
L_6	1.1	T_1	0.8
L_7	1.6	D_1	23.5
L_8	1.25	D_2	16.75
L_9	3.2	D_3	3.88
L_{10}	1.54	D_4	0.8
L_{11}	2.7	D_5	0.38

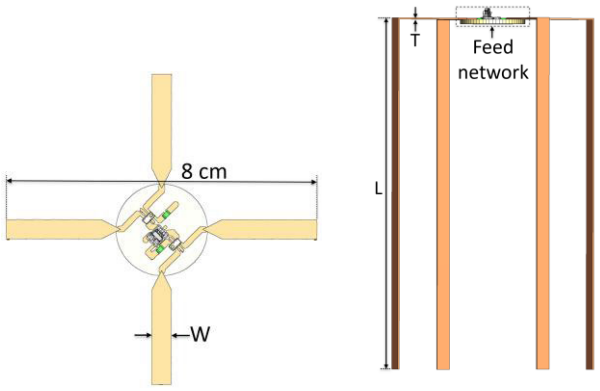

(a) (b)

FIGURE 4. 3D bent cross dipole antenna design for englacial and subglacial probe applications, (a) Top view, (b) Side view.

C. BENT CROSS DIPOLE ANTENNA FOR ENGLACIAL SENSOR PROBE

Conventionally, a crossed dipole or turnstile antenna [51] is planar with the four branches on a 2D plane. The branches usually at right angles to the adjacent ones give a square shape to the antenna with each side approximately 0.5 λ_e. At 433 MHz, 0.5 λ_e= 0.5 x $\frac{c_{/f}}{\sqrt{\varepsilon_r}}$ = 19.5 cm, while the available space in the sensor probe is only 0.2 λ_e or 8 cm. To cater for this size constraint, the antenna branches were bended after they occupied the available 0.2 λ_e space radially. The basic antenna design is shown in Fig. 4. The antenna comprises four branches of annealed copper. Each branch has a horizontal and a vertical segment. The vertical segment increases the effective length of the antenna since the horizontal length cannot exceed 8 cm. The transceiver signal is inputted to a feed network that acts as a power splitter and a phase shifter. The 0°, 90°, 180°, and 270° phase signals from the feed network feed each of the four branches of the antenna in a CCW sequence. This makes the antenna LHCP. The antenna was simulated using Computer simulation technology (CST) studio software. The presence of other electronics in the sensor probe including batteries were catered for in the simulations.

(a) (b)

FIGURE 5. Developed 3D bent cross dipole antenna for englacial probe applications, (a) With a support ring, (b) Installed in actual sensor probe.

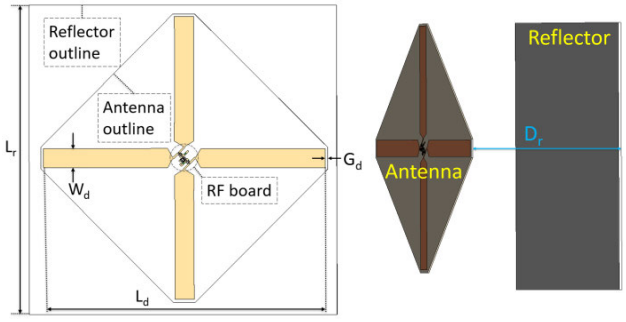

(a) (b)

FIGURE 6. Design of the planar printed cross dipole antenna for glacier surface receiver applications, (a) Top view, (b) Perspective view.

The developed antenna is shown in Fig. 5(a). The purpose of the yellow ring in Fig. 5(a) is to keep the antenna branches apart at the correct separation and is not used in the actual installation. The 3D bent cross dipole antenna installed in the sensor probe assembly is shown in Fig. 5(b).

D. PLANAR PRINTED CROSS DIPOLE ANTENNA FOR GLACIER SURFACE RECEIVERS

From the link budget calculations in the previous section, the surface RX antenna had to provide a minimum realized gain of 5 dBic. Usually, the maximum realized gain a cross dipole antenna can provide is 2.5 dBic [51]. A typical cross dipole antenna is bi-directional with symmetric far fields on both the broadsides. Since the surface antenna only needed to receive from one direction, a quarter-wave reflector was placed on the top side to make it unidirectional with a higher gain. The same feed network, as used for the 3D bent cross dipole, was used making the antenna LHCP. The antenna design is shown in Fig. 6. The antenna branches printed on a 0.8 mm FR-4 board ($\varepsilon_r = 4.3$, $\tan\delta = 0.025$) were tapered where they joined the feed network to avoid reflections and maintain a good signal quality. The reflector was placed at $D_r = \frac{\lambda}{4}$ distance from the antenna. The antenna was designed and optimized using CST studio suite software. The geometric parameters of the antenna are $L_d = 26.72$ cm, $W_d = 1.81$ cm, $G_d = 0.32$ cm, $L_r = 51.96$ cm, and $D_r = 17.32$ cm. The developed antenna is shown in Fig. 7.

FIGURE 7. Developed planar printed cross dipole antenna for glacier surface receiver applications.

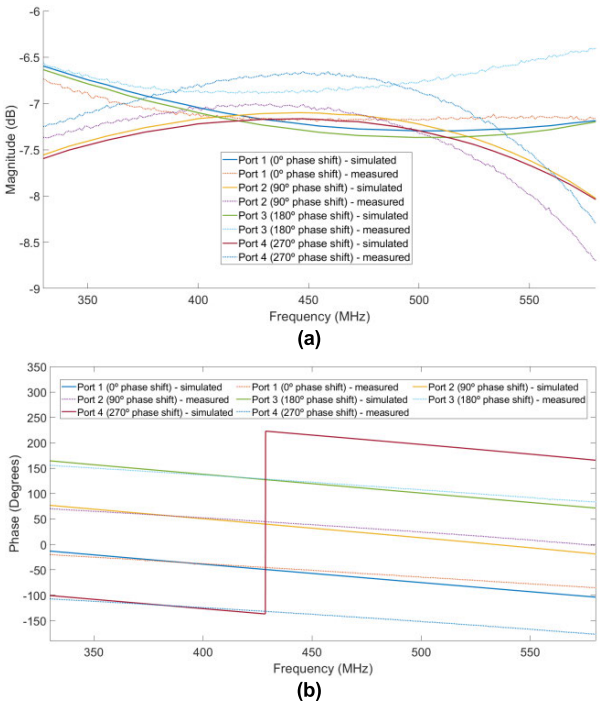

(a)

(b)

FIGURE 8. Feed network results, (a) Simulated and measured signal amplitudes from the four ports, (b) Simulated and measured phases of the four port signals.

V. PARAMETRIC STUDY AND RESULTS

A. FEED NETWORK

The desirable response from the feed network was good amplitude and phase balance. Simulations were done in ADS software, while experimental measurements were made using

a vector network analyzer. For experimental measurements, the test feed network shown in Fig. 3 was used. When measuring the output from one port, the remaining three ports were terminated using 50 Ω terminations. The simulated and measured signal amplitudes from the four ports are shown in Fig 8(a). Ports 1, 2, 3, and 4 have phases of 0°, 90°, 180°, and 270° respectively. At the center frequency of 433 MHz, the simulated and measured amplitude imbalances were 0.15 dB and 0.48 dB respectively. Amplitude imbalance here refers to the maximum difference in amplitude between any of the four ports. An amplitude imbalance of less than half a decibel at 433 MHz shows a good quality of amplitude balance. The 0.5 dB amplitude imbalance fractional bandwidth (AI-FBW) was measured as $\frac{f_h - f_l}{fc} \times 100$ where f_l and f_h represent the lowest and highest frequencies between which the amplitude imbalance remains below 0.5 dB. The center frequency is represented by $f_c = 433$ MHz. Simulated and measured 0.5 dB AI-FBWs remained 43% (between 372 MHz and 558 MHz) and 32% (from 357 MHz to 496 MHz) respectively. The simulated and measured 1 dB AI-FBWs remained 57% (between 330 MHz to 580 MHz which represents the complete measurement range) and 46 % (between 330 MHz to 530 MHz) respectively. These measurements suggest that the feed network could be used for designing cross dipole antennas operating in the range between 330 to 530 MHz since an amplitude imbalance of up to 1 dB is usually acceptable for such antenna designs. The measured amplitude imbalance gradually increased beyond 1 dB from 530 MHz onwards reaching a maximum of 2.29 dB at 580 MHz. The relatively higher amplitude imbalance between 530 MHz to 580 MHz is attributed to the hybrid ICs' poor performance in the 530-580 MHz range, and fabrication and experimental errors.

Ideally, a 90° phase difference should be maintained across all the adjacent ports of the feed network. Phase imbalance refers to deviation in degrees from 90° phase difference across any two adjacent ports. From Fig. 8(b), the mean simulated and measured phase imbalances remained 2.4° and 4.6° respectively. The maximum simulated and measured phase imbalances at any point in the complete frequency range were 4.5° and 6° respectively. This shows a good agreement between the simulated and measured results, as well as a good quality of phase balance which can facilitate high quality of antenna circular polarization.

B. BENT CROSS DIPOLE ANTENNA

1) PARAMETRIC STUDY

Parametric study was carried out for the following purposes:

- To see the effect of changing antenna length L, width W and thickness T on the antenna performance metrics including the realized gain, and axial ratio.
- To maximize the realized gain at 433 MHz while maintaining a -10 dB $|S_{11}|$ bandwidth of at least a few tens of MHz. The optimization variables were L, W, and T. The optimization constraint was that the combined horizontal length of two opposite facing arms could not exceed 8 cm. This constraint was derived from the maximum available borehole size.

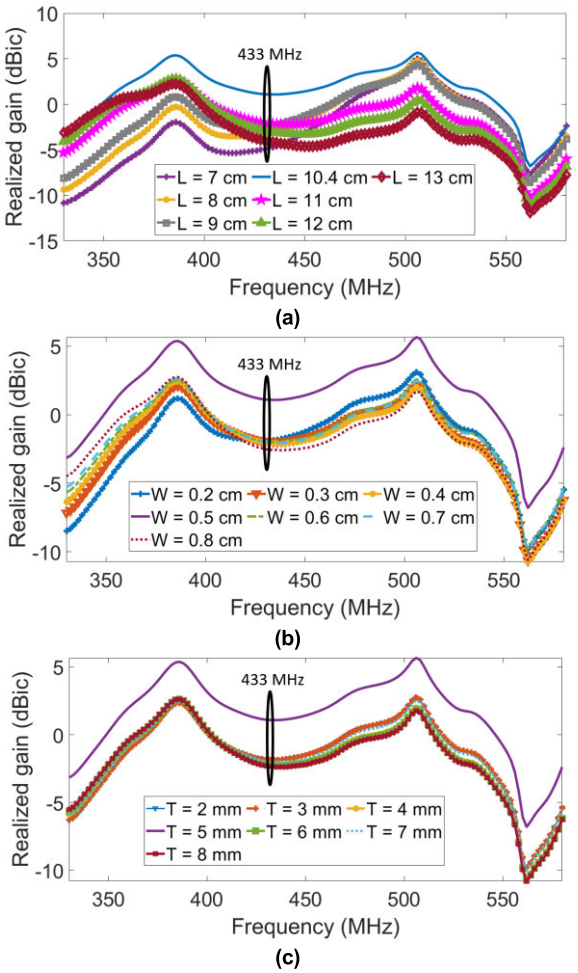

FIGURE 9. Parameter sweep results for the bent cross dipole antenna. (a), (b), and (c) show the effect of changing antenna length L, width W, and thickness T on the realized gain respectively. In (a), W and T were kept constant at 0.5 cm and 5 mm respectively. In (b), L and T were kept constant at 10.4 cm and 5 mm respectively. In (c), L and W were kept constant at 10.4 cm and 0.5 cm respectively.

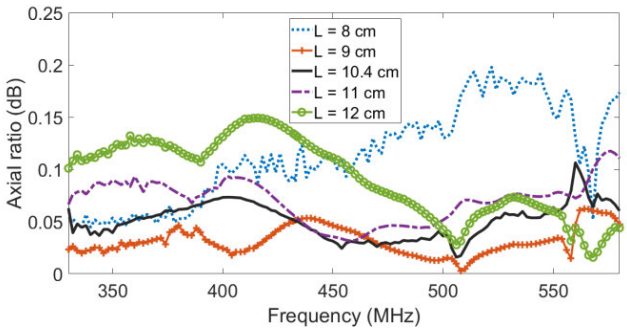

FIGURE 10. The bent cross dipole antenna axial ratio versus frequency for different values of L with fixed $W = 0.5$ cm and $T = 5$ mm.

The parameters L, W, and T are shown in Fig. 4. One parameter was varied at a time while keeping the other two fixed. Figs 9(a), 9(b), and 9(c) show the effect of changing parameters L, W, and T on the antenna's realized gain. The

TABLE 5. Optimum parameters of the bent cross dipole antenna.

Parameter	L	W	T
Value	10.4 cm	0.5 cm	5 mm

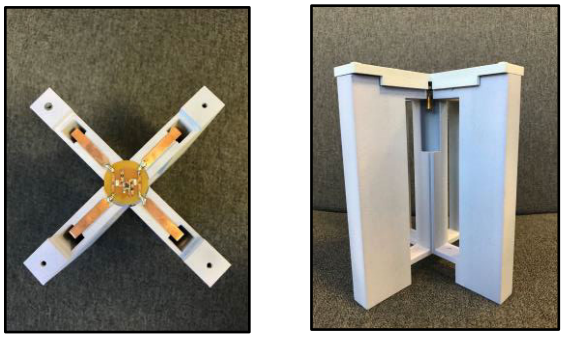

(a) (b)

FIGURE 11. Custom designed and made Nylon casing for the 3D bent cross dipole antenna to facilitate free space testing, (a) Top view without cover, (b) Side view with top cover.

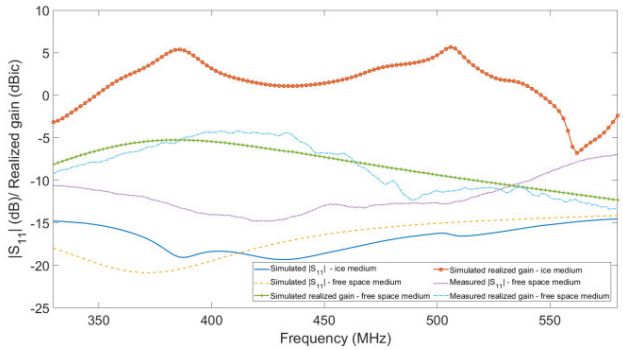

FIGURE 12. Simulated and measured $|S_{11}|$ and realized gain of the 3D bent cross dipole antenna in snow and free space media.

optimum parameters thus found are shown in Table 5 and provided a realized gain of 1 dBic at 433 MHz in ice. The simulated axial ratio remained under 0.25 dB across the 330- 580 MHz frequency range for all the selected values of L, W, and T. This is attributed to the symmetric design of the antenna. The axial ratio for different values of L with fixed $W = 0.5$ cm and $T = 5$ mm is shown in Fig. 10.

2) RESULTS

The available lab resources did not permit in-ice testing of the antenna. A substitute experimental validation method was thus used. Simulations were performed in ice and free space media, followed by practical testing of a version of the antenna in free space. If the simulation and experimental results in free space medium agreed well, we can confidently expect the antenna to perform in ice medium in line with the ice medium simulations. To facilitate safe testing of the bent cross dipole antenna in free space, a nylon ($\varepsilon_r = 3.8$) antenna casing was made. The purpose of the casing was firstly to provide structural support to the antenna, and secondly to facilitate antenna testing by providing for the antenna to be fixed in position at the antenna test range. The antenna

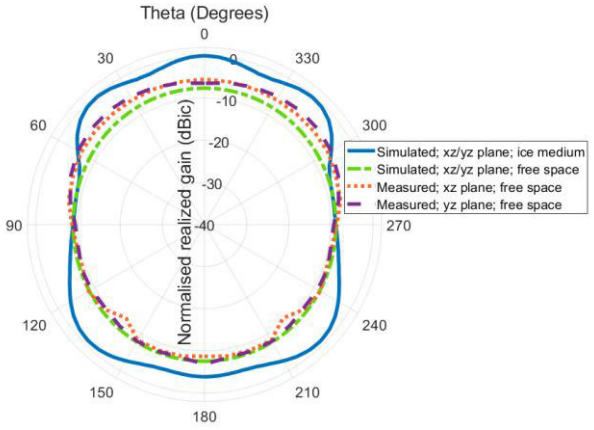

FIGURE 13. Simulated and measured radiation patterns of the bent cross dipole antenna in xz/ E-plane and yz/ H-plane at 433 MHz.

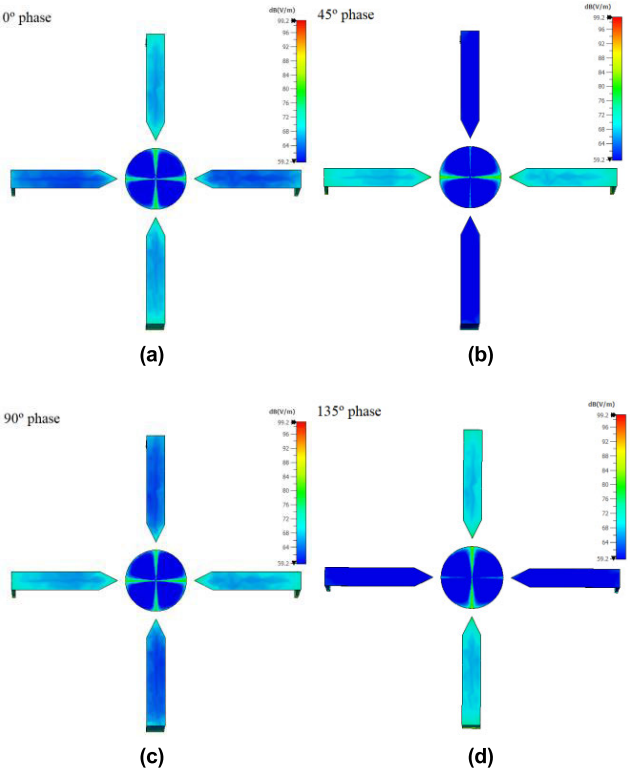

FIGURE 14. E-field contour plots of the 3D bent cross dipole antenna at 433 MHz with different phases of the excitation signal, (a) 0° phase, (b) 45° phase, (c) 90° phase, (d) 135° phase.

installed in the nylon casing is shown in Fig. 11. It must be noted here that the casing material (nylon) affects the radiation characteristics of the antenna. The antenna performance in free space, especially the realized gain would be better without the nylon casing. However, the important thing is that the simulation and measured results in free space should agree.

Simulated and measured results of the bent cross dipole antenna in ice ($\varepsilon_r = 3.1$) and free space media are shown in Figs. 12 to 18. From Fig. 12, the antenna provides a -10 dB fractional bandwidth (FBW) of 57% while operating at a center frequency of 433 MHz in ice. The realized gain

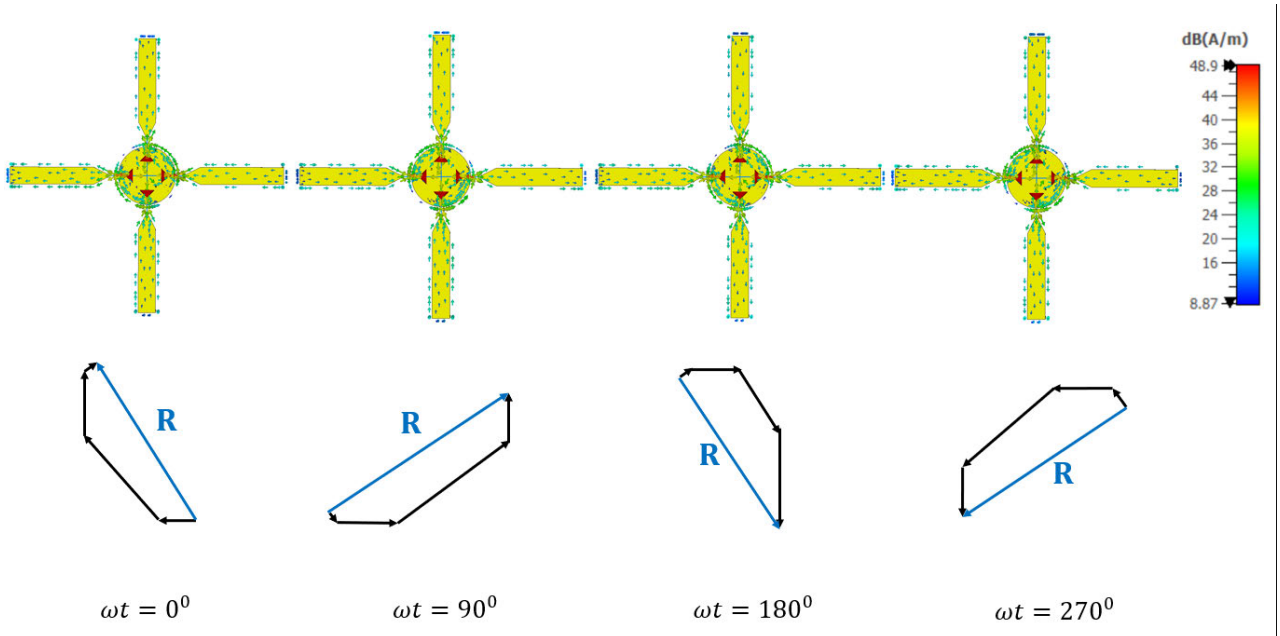

FIGURE 15. Surface current distribution on the 3D bent cross dipole antenna for different phase angles at 433 MHz.

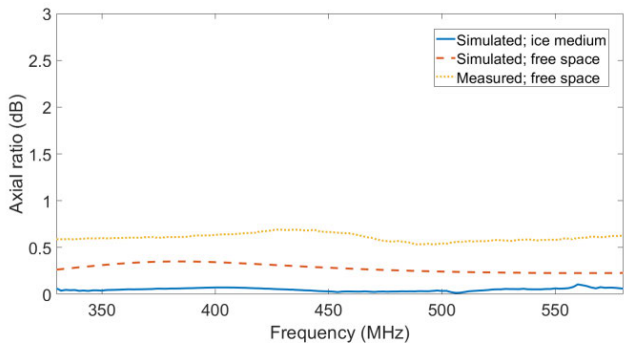

FIGURE 16. Simulated and measured axial ratios of the 3D bent cross dipole antenna in ice and free space media.

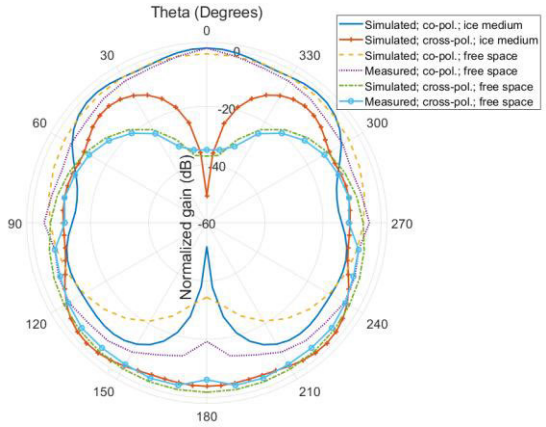

FIGURE 17. Ice and free space media simulated and measured co- and cross polarization radiation patterns of the 3D bent cross dipole antenna at 433 MHz in xz/ E-plane.

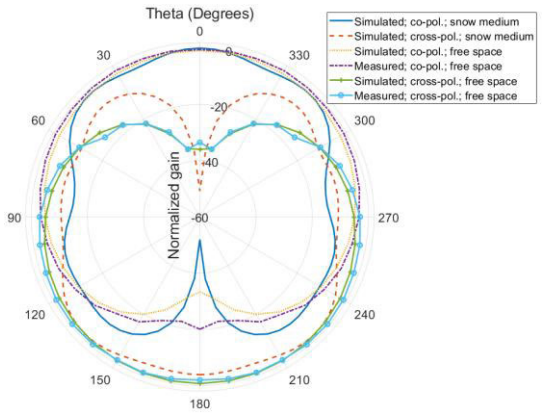

FIGURE 18. Ice and free space media simulated and measured co- and cross polarization radiation patterns of the 3D bent cross dipole antenna at 433 MHz in yz/ H-plane.

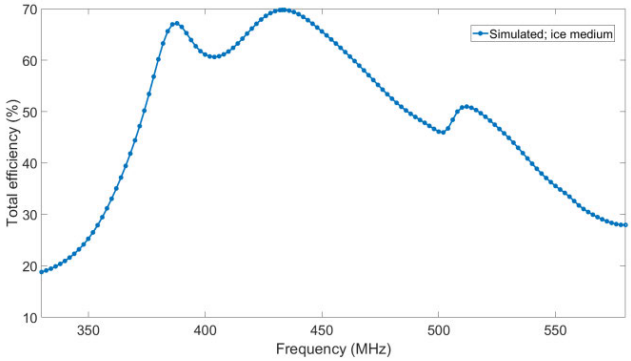

FIGURE 19. Total efficiency of the 3D bent cross dipole antenna in ice medium.

in ice at 433 MHz as shown in Fig. 12 is 1 dBic with a large 3 dB gain bandwidth of 49%. The simulated and measured $|S_{11}|$ and realized gain in free space also shown in Fig. 12 are in satisfactory agreement. The simulated and

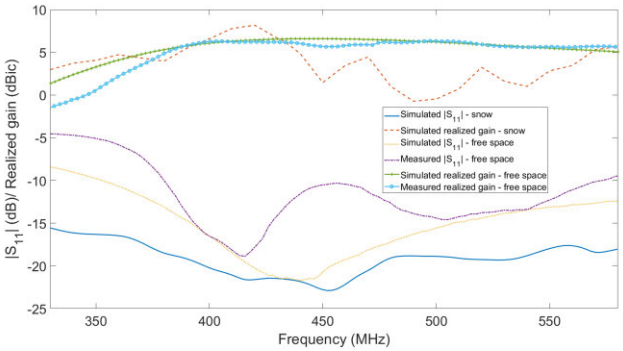

FIGURE 20. Simulated and measured |S11| and realized gain of the planar printed cross dipole antenna in snow and free space media.

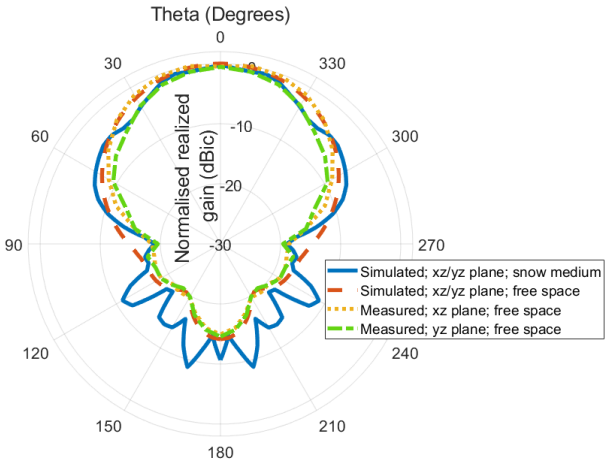

FIGURE 21. Snow and free space media simulated and measured radiation patterns of the planar printed cross dipole antenna at 433 MHz in xz/ E-plane and yz/ H-plane.

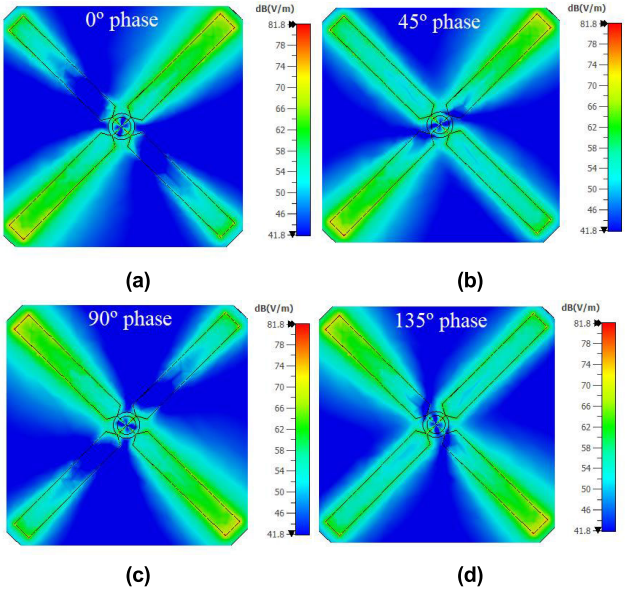

FIGURE 22. E-field contour plots of the planar printed cross dipole antenna at 433 MHz with different phases of the excitation signal, (a) 0° phase, (b) 45° phase, (c) 90° phase, (d) 135° phase.

measured -10 dB FBWs in free space remained 57% and 48% respectively. Some differences between the simulation and measured results are attributed to antenna fabrication and experimental errors. Due to symmetric design of the antenna, the simulated far field patterns in the xz/ E-plane (Phi = 0°) and yz/ H-plane (Phi = 90°) are the same. The simulated and measured radiation patterns in xz and yz planes in both ice and free space media are plotted in Fig. 13. The antenna provides half power beamwidths (HPBWs) of 108° in both the vertical planes xz and yz in ice which is well above the desired HPBW of 50° and will cater well for the TX-RX antenna misalignments due to basal sliding occurring over extended deployments. The simulated and measured far field patterns in free space also presented in Fig. 13 are in good agreement. Fig. 14 shows the E-field contour plots for different phases. Rotation of the E-field in Fig. 14 shows the circular polarization of the antenna. The mechanism of CP can be better understood by analyzing the surface current distribution at different phases. Surface current directions on the antenna for different phases ($\omega t = 0^0, 90^0, 180^0, 270^0$) are shown in Fig. 15. The resultant surface current direction has been found using composite vector analysis [53], [54] and shown by the blue colored resultant vector **R** for each phase. The clockwise (CW) rotation of the vector **R** with respect to the phase angle validates the left hand CP (LHCP) of the antenna.

The simulated and measured axial ratios in ice and free space mediums are plotted in Fig. 16. The simulated axial ratios in ice and free space media both remained below 0.3 dB over the complete frequency measurement range 330-580 MHz and shows an excellent quality of circular polarization. The free space measured axial ratio remained below 0.6 dB over the 330-580 MHz frequency and the mean difference between the free space simulated and measured axial ratios remained 0.32 dB. The simulated and measured 3 dB axial ratio bandwidths (ARBW) were measured as 54.9%. Again, due to the symmetry in antenna design, the simulated co- and cross-polarizations in both xz and yz planes remained the same. The co- and cross-polarization radiation patterns in xz-plane are plotted in Fig. 17. From Fig. 17, the ice medium co-polarization is $>$ 40 dB stronger than the cross polarization in $\theta = 0^0, \varphi = 0^0$ direction. The ice medium co-polarization is stronger than cross-polarization by at least 12 dB within a beamwidth of 40° at 433 MHz. This shows good rejection of RHCP radiation and an adequate purity of antenna polarization. The measured purity of antenna polarization also remained very good. Within a beam width of 60° in the xz plane, the free space measured co-polarization remained stronger by at least 20.9 dB than the cross-polarization while the maximum difference between the co and cross polarization was noted in the $\theta = 0^0, \varphi = 0^0$ direction as 31.6 dB. The ice and free space media co- and cross polarizations in yz plane are similarly shown in Fig. 18. While the simulated plots are the same as in Fig. 17 due to antenna symmetry, the difference between the measured co and cross polarization in the yz plane ($\theta = 0^0, \varphi = 90^0$) remained 33 dB. The free space measured co-polarization remained stronger by at least 20.3 dB than the

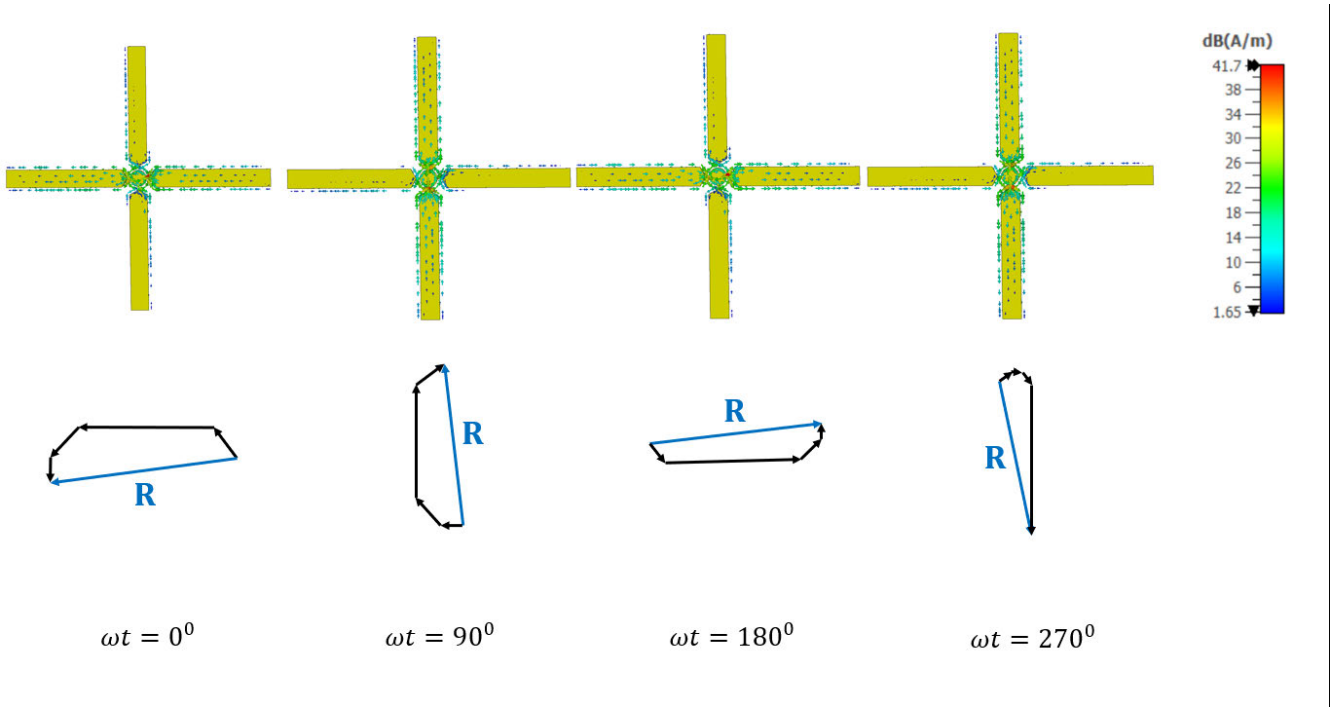

FIGURE 23. Surface current distribution on the planar printed cross dipole antenna for different phase angles at 433 MHz.

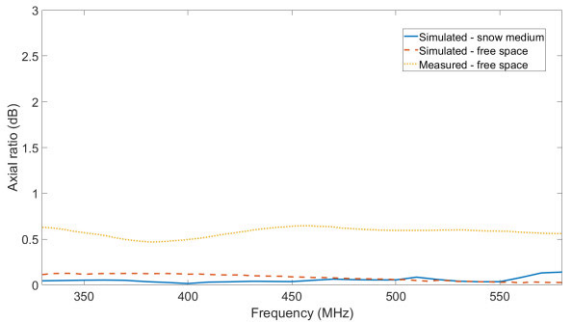

FIGURE 24. Simulated and measured axial ratios of the planar printed cross dipole antenna in snow and free space media.

cross polarization within a beam width of 60° in the yz plane. From Fig. 19, the antenna provides a 69.7 % total efficiency at 433 MHz which is an acceptable figure for an electrically small antenna like the 3D bent cross dipole.

C. PLANAR PRINTED CROSS DIPOLE ANTENNA

A similar testing methodology like used for the 3D bent cross dipole antenna was used here. A good agreement between the free space simulations and experimental measurements was observed, thus validating the snow medium simulation results. The antenna has a -10 dB FBW of 57% with the |S11| remaining below -15 dB between 330 to 580 MHz in snow ($\varepsilon_r = 2.5$). The |S11| as well as the realized gain in snow are plotted in Fig. 20. At the operating frequency of 433 MHz, the antenna realized gain in snow was noted as 6.1 dBic. This is 1.1 dBic above the required gain of 5 dBic and therefore offers some additional link margin. The gain remained above 5 dBic between 387 – 439 MHz and 568 – 580 MHz, which makes the antenna a good choice if the operating frequency lies within the aforesaid ranges. Nevertheless, the gain remains above 0 dBic almost across the complete range 330 – 580 MHz making it suitable for less gain demanding applications as well. The simulated and measured $|S_{11}|$ and realized gain of the printed cross dipole antenna in free space medium are also plotted in Fig. 20. The simulated and measured -10 dB FBWs in free space remained 52% and 45% respectively. The simulated and measured gain in free space match satisfactorily. Some differences in the simulated and measured results, especially in the frequency range 330 – 370 MHz are attributed to fabrication imperfections and experimental errors. The symmetrical design of the antenna resulted in identical simulated radiation patterns in both the xz and yz planes as shown in Fig. 21. The HPBW of the antenna in both the planes in snow was 60°, thus satisfying the Thwaites project requirement of 50°. Free space simulated and measured radiation patterns in the xz and yz planes plotted in Fig. 21 agree well. From Fig 21, the xz plane simulated and measured HPBWs in free space remained 76° and 82° respectively, while the yz plane simulated and measured HPBWs were noted as being 76° and 62° respectively. The E-field contour plots of Fig. 22 at different phases of the excitation signal show the circular polarization of the antenna. Fig. 23 demonstrates the mechanism of LHCP where the resultant surface current direction (shown by vector **R**) [53], [54] has been shown for different phase angles. The CW rotation of vector **R** in relation to the phase angle proves LHCP of the antenna. From Fig. 24, the simulated axial ratios in both snow and free space media remained below 0.2 dB,

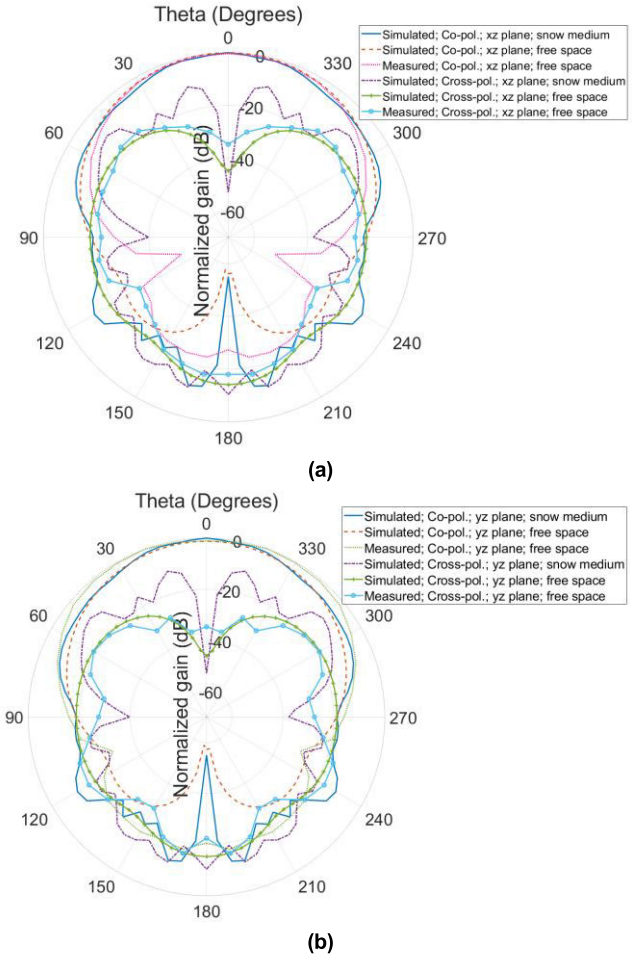

FIGURE 25. Snow and free space media simulated and measured co- and cross polarization radiation patterns of the planar printed cross dipole antenna at 433 MHz, (a) xz/ E-plane, (b) yz/ H plane.

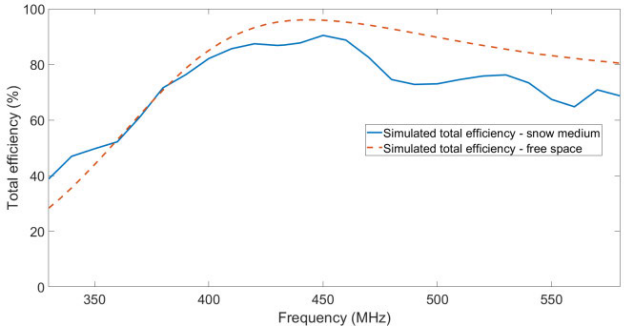

FIGURE 26. Total efficiency of the planar printed cross dipole antenna in snow and free space media.

while the free space measured axial ratio stood below 0.7 dB across 330 to 580 MHz. This proves an excellent quality of circular polarization making the antenna well resistant to reception losses due to orientation errors. The mean difference between free space simulated and measured axial ratios remained 0.49 dB. The ARBW of the antenna remained at 54.9%. From Figs. 25(a) and 25(b), the snow medium co-polarization radiation is stronger than the cross-polarization by at least 20 dB within a beamwidth of 10° (5° on either side of the $\theta = 0°$ direction) in xz/ yz planes. Within a beamwidth of 60° in snow, the co-polarization remained stronger by at least 10 dB than the cross- polarization in both the xz and yz planes. This shows satisfactory purity of polarization. From Fig. 25(a), the free space simulated and measured differences between co and cross polarizations in xz-plane at 433 MHz remained at least 21 dB and 20 dB respectively within a beam width of 60° showing a close match. From Fig. 25(b), the simulated and measured differences between the free space co and cross polarization in the yz-plane remained at least 30 dB and 21 dB respectively within a beam width of 60°. The antenna provides a good total efficiency of 86.9% at the operating frequency of 433 MHz in snow as shown in Fig. 26.

VI. CONCLUSION

A link budget framework for calculating antenna parameters of a glacial environmental sensor network (ESN) has been presented and explained with the help of an example. Designs of two antennas developed for the Thwaites project are also presented. The Thwaites project aims to deploy a glacial ESN at the Thwaites glacier, Antarctica. The developed antennas cater for challenges of performing in ice and snow for extended deployments as well as meet requirements specific to the Thwaites project. The state-of-the-art works either used a helical, coil ferrite, or a dielectric resonator antenna for englacial probes. This work has designed and assessed a 3D bent cross dipole antenna for use in sensor probes. The 3D bent cross dipole antenna fits in a sensor probe of just 8 cm diameter while providing a gain of 1 dBic at 433 MHz. The kinds of antennas previously used with surface RXs included Yagi, helical, non-printed cross dipole, and log periodic dipole array. This work has developed and validated a printed cross dipole antenna for use with surface RXs. The antenna provides a gain of 6.1 dBic at 433 MHz. The two antennas together provide an additional link margin of 2.1 dB above the Thwaites project requirements. The Thwaites project requires the antennas to provide half power beamwidths (HPBWs) of at least 50° in the planes xz and yz at 433 MHz. Both the developed antennas meet the HPBW requirements, with the 3D bent cross dipole and the printed cross dipole antennas providing HPBWs of 108° and 60° respectively at 433 MHz in both the vertical planes xz and yz. The two antennas show excellent circular polarization traits and their measured axial ratios remained below 0.7 dB between 330-580 MHz. The antennas' beamwidths and axial ratios cater well for misalignments between the ESN TX-RX antennas expected over extended deployments. The antennas' co-polarizations remained stronger by at least 10 dB than the cross polarizations in both the vertical planes within a beamwidth of 40° and shows adequate purity of antennas' LHCP. Lastly, the previous glacial ESNs used frequencies below 433 MHz for achieving communication ranges above a hundred metres. This paper has theoretically proved and experimentally validated the 433 MHz band for achieving englacial communication ranges up to 2300 metres.

REFERENCES

[1] S. Marshall, *The Cryosphere*. Princeton, NJ, USA: Princeton Univ. Press, 2012.

[2] S. S. Jacobs, H. H. Helmer, C. S. M. Doake, A. Jenkins, and R. M. Frolich, "Melting of ice shelves and the mass balance of Antarctica," *J. Glaciol.*, vol. 38, no. 130, pp. 375–387, 1992, doi: 10.3189/S0022143000002252.

[3] A. S. Trupin, M. F. Meier, and J. M. Wahr, "Effect of melting glaciers on the Earth's rotation and gravitational field: 1965–1984," *Geophys. J. Int.*, vol. 108, no. 1, pp. 1–15, Jan. 1992, doi: 10.1111/J.1365-246X.1992.TB00835.X.

[4] J. Xu, R. E. Grumbine, A. Shrestha, M. Eriksson, X. Yang, Y. Wang, and A. Wilkes, "The melting Himalayas: Cascading effects of climate change on water, biodiversity, and livelihoods," *Conserv. Biol.*, vol. 23, no. 3, pp. 520–530, Jun. 2009, doi: 10.1111/J.1523-1739.2009.01237.X.

[5] M. Carey, *In the Shadow of Melting Glaciers: Climate Change and Andean Society*. Oxford, U.K.: Oxford Univ. Press, 2010, doi: 10.1093/ACPROF:OSO/9780195396065.001.0001.

[6] C. A. Katsman, W. Hazeleger, S. S. Drijfhout, G. J. van Oldenborgh, and G. Burgers, "Climate scenarios of sea level rise for the northeast Atlantic Ocean: A study including the effects of ocean dynamics and gravity changes induced by ice melt," *Climatic Change*, vol. 91, nos. 3–4, pp. 351–374, Aug. 2008, doi: 10.1007/S10584-008-9442-9.

[7] J. M. Gregory and J. Oerlemans, "Simulated future sea-level rise due to glacier melt based on regionally and seasonally resolved temperature changes," *Nature*, vol. 391, no. 6666, pp. 474–476, Jan. 1998, doi: 10.1038/35119.

[8] J. Hansen, M. Sato, P. Hearty, R. Ruedy, M. Kelley, V. Masson-Delmotte, G. Russell, G. Tselioudis, J. Cao, E. Rignot, I. Velicogna, B. Tormey, B. Donovan, E. Kandiano, K. von Schuckmann, P. Kharecha, A. N. Legrande, M. Bauer, and K.-W. Lo, "Ice melt, sea level rise and superstorms: Evidence from paleoclimate data, climate modeling, and modern observations that 2 °C global warming could be dangerous," *Atmos. Chem. Phys.*, vol. 16, no. 6, pp. 3761–3812, Mar. 2016, doi: 10.5194/ACP-16-3761-2016.

[9] S. R. Bajracharya, P. K. Mool, and B. R. Shrestha, "Global climate change and melting of Himalayan glaciers," in *Melting Glaciers and Rising Sea Levels: Impacts and Implications*. Hyderabad, India: Icfai Univ. Press, 2008, pp. 28–46.

[10] U. Mikolajewicz, M. Vizcaíno, J. Jungclaus, and G. Schurgers, "Effect of ice sheet interactions in anthropogenic climate change simulations," *Geophys. Res. Lett.*, vol. 34, no. 18, Sep. 2007, Art. no. L18706, doi: 10.1029/2007GL031173.

[11] K. Martinez, J. K. Hart, and R. Ong, "Environmental sensor networks," *Computer*, vol. 37, no. 8, pp. 50–56, Aug. 2004, doi: 10.1109/MC.2004.91.

[12] J. K. Hart, K. Martinez, R. Ong, A. Riddoch, K. C. Rose, and P. Padhy, "A wireless multi-sensor subglacial probe: Design and preliminary results," *J. Glaciol.*, vol. 52, no. 178, pp. 389–397, 2006, doi: 10.3189/172756506781828575.

[13] K. C. Rose, J. K. Hart, and K. Martinez, "Seasonal changes in basal conditions at Briksdalsbreen, Norway: The winter-spring transition," *Boreas*, vol. 38, no. 3, pp. 579–590, Aug. 2009, doi: 10.1111/J.1502-3885.2008.00079.X.

[14] K. Martinez, J. K. Hart, and R. Ong, "Deploying a wireless sensor network in Iceland," in *Proc. Int. Conf. GeoSensor Netw.* Berlin, Germany: Springer, 2009, pp. 131–137, doi: 10.1007/978-3-642-02903-5_13.

[15] K. Martinez and P. Basford, "Robust wireless sensor network performance analysis," *Proc. IEEE Sensors*, pp. 203–206, Oct. 2011, doi: 10.1109/ICSENS.2011.6127105.

[16] J. K. Hart, K. C. Rose, R. I. Waller, D. Vaughan-Hirsch, and K. Martinez, "Assessing the catastrophic break-up of Briksdalsbreen, Norway, associated with rapid climate change," *J. Geol. Soc. London*, vol. 168, no. 3, pp. 673–688, May 2011, doi: 10.1144/0016-76492010-024.

[17] J. K. Hart, K. C. Rose, A. Clayton, and K. Martinez, "Englacial and subglacial water flow at Skálafellsjökull, Iceland derived from ground penetrating radar, in situ Glacsweb probe and borehole water level measurements," *Earth Surf. Process. Landforms*, vol. 40, no. 15, pp. 2071–2083, Dec. 2015, doi: 10.1002/ESP.3783.

[18] K. Martinez, J. K. Hart, P. J. Basford, G. M. Bragg, T. Ward, and D. S. Young, "A geophone wireless sensor network for investigating glacier stick-slip motion," *Comput., Geosci.*, vol. 105, pp. 103–112, Aug. 2017, doi: 10.1016/J.CAGEO.2017.05.005.

[19] C. J. P. P. Smeets, W. Boot, A. Hubbard, R. Pettersson, F. Wilhelms, M. R. Van Den Broeke, and R. S. W. Van De Wal, "A wireless subglacial probe for deep ice applications," *J. Glaciol.*, vol. 58, no. 211, pp. 841–848, 2012, doi: 10.3189/2012JOG11J130.

[20] P. How, D. I. Benn, N. R. J. Hulton, B. Hubbard, A. Luckman, H. Sevestre, W. J. J. van Pelt, K. Lindbäck, J. Kohler, and W. Boot, "Rapidly changing subglacial hydrological pathways at a tidewater glacier revealed through simultaneous observations of water pressure, supraglacial lakes, meltwater plumes and surface velocities," *Cryosphere*, vol. 11, no. 6, pp. 2691–2710, Nov. 2017, doi: 10.5194/TC-11-2691-2017.

[21] E. A. Bagshaw, S. Burrow, J. L. Wadham, J. Bowden, B. Lishman, M. Salter, R. Barnes, and P. Nienow, "E-tracers: Development of a low cost wireless technique for exploring sub-surface hydrological systems," *Hydrol. Process.*, vol. 26, no. 20, pp. 3157–3160, Sep. 2012, doi: 10.1002/HYP.9451.

[22] E. A. Bagshaw, B. Lishman, J. L. Wadham, J. A. Bowden, S. G. Burrow, L. R. Clare, and D. Chandler, "Novel wireless sensors for in situ measurement of sub-ice hydrologic systems," *Ann. Glaciol.*, vol. 55, no. 65, pp. 41–50, 2014, doi: 10.3189/2014AOG65A007.

[23] E. A. Bagshaw, N. B. Karlsson, L. B. Lok, B. Lishman, L. Clare, K. W. Nicholls, S. Burrow, J. L. Wadham, O. Eisen, H. Corr, P. Brennan, and D. Dahl-Jensen, "Prototype wireless sensors for monitoring subsurface processes in snow and firn," *J. Glaciol.*, vol. 64, no. 248, pp. 887–896, Dec. 2018, doi: 10.1017/JOG.2018.76.

[24] W. D. Harrison, M. Truffer, K. A. Echelmeyer, D. A. Pomraning, K. A. Abnett, and R. H. Ruhkick, "Probing the till beneath Black Rapids Glacier, Alaska, USA," *J. Glaciol.*, vol. 50, no. 171, pp. 608–614, 2004, doi: 10.3189/172756504781829693.

[25] A. Behar, H. Wang, A. Elliot, S. O'Hern, C. Lutz, S. Martin, K. Steffen, D. McGrath, and T. Phillips, "The moulin explorer: A novel instrument to study Greenland ice sheet melt-water flow," in *Proc. IOP Conf. Ser., Earth Environ. Sci.*, vol. 6, no. 1, Jan. 2009, Art. no. 012020, doi: 10.1088/1755-1307/6/1/012020.

[26] A. Petosa, A. Ittipiboon, Y. M. M. Antar, D. Roscoe, and M. Cuhaci, "Recent advances in dielectric-resonator antenna technology," *IEEE Antennas Propag. Mag.*, vol. 40, no. 3, pp. 35–47, Jun. 1998, doi: 10.1109/74.706069.

[27] B. Mukherjee, P. Patel, and J. Mukherjee, "A review of the recent advances in dielectric resonator antennas," *J. Electromagn. Waves Appl.*, vol. 34, no. 9, pp. 1095–1158, Jun. 2020, doi: 10.1080/09205071.2020.1744484.

[28] A. R. Djordfevic, A. G. Zajic, M. M. Ilic, and G. L. Stuber, "Optimization of helical antennas [antenna designer's notebook]," *IEEE Antennas Propag. Mag.*, vol. 48, no. 6, pp. 107–115, Dec. 2006, doi: 10.1109/MAP.2006.323359.

[29] N. J. G. Fonseca and H. Aubert, "Compact helical antennas—A review," *Recent Patents Elect., Electron. Eng., Formerly Recent Patents Elect. Eng.*, vol. 3, no. 1, pp. 1–9, 2010.

[30] S. R. Best, "A discussion on the properties of electrically small self-resonant wire antennas," *IEEE Antennas Propag. Mag.*, vol. 46, no. 6, pp. 9–22, Dec. 2004, doi: 10.1109/MAP.2004.1396731.

[31] S. R. Best and D. L. Hanna, "A performance comparison of fundamental small-antenna designs," *IEEE Antennas Propag. Mag.*, vol. 52, no. 1, pp. 47–70, Feb. 2010, doi: 10.1109/MAP.2010.5466398.

[32] H. Lei, Y. Liu, Y. Jia, Z. Yue, and X. Wang, "A low-profile dual-band dual-circularly polarized folded transmitarray antenna with independent beam control," *IEEE Trans. Antennas Propag.*, vol. 70, no. 5, pp. 3852–3857, May 2022, doi: 10.1109/TAP.2021.3125419.

[33] Y. Yan, Y. Jiao, H. Cheng, and C. Zhang, "A low-profile dual-circularly polarized wide-axial-ratio-beamwidth slot patch antenna with six-port feeding network," *IEEE Antennas Wireless Propag. Lett.*, vol. 20, no. 12, pp. 2486–2490, Dec. 2021, doi: 10.1109/LAWP.2021.3115802.

[34] S. Chen, R. W. Ziolkowski, B. Jones, and Y. J. Guo, "Analysis, design, and measurement of directed-beam toroidal waveguide-based leaky-wave antennas," *IEEE Trans. Antennas Propag.*, vol. 70, no. 11, pp. 10141–10155, Nov. 2022, doi: 10.1109/TAP.2022.3191126.

[35] Z. Wang and Y. Dong, "Circularly polarized antennas inspired by dual-mode SIW cavities," *IEEE Access*, vol. 7, pp. 173007–173018, 2019, doi: 10.1109/ACCESS.2019.2956750.

[36] Z. Chen, W. Hu, Y. Gao, L. Wen, C. Li, Z. Hu, W. Jiang, and S. Gao, "Compact wideband circularly polarized loop antenna based on dual common and differential modes," *IEEE Antennas Wireless Propag. Lett.*, vol. 21, no. 8, pp. 1567–1571, Aug. 2022, doi: 10.1109/LAWP.2022.3174400.

[37] R. Xu, J. Liu, K. Wei, W. Hu, Z. Xing, J. Li, and S. S. Gao, "Dual-band circularly polarized antenna with two pairs of crossed-dipoles for RFID reader," *IEEE Trans. Antennas Propag.*, vol. 69, no. 12, pp. 8194–8203, Dec. 2021, doi: 10.1109/TAP.2021.3083827.
[38] L. Wen, S. Gao, Q. Luo, W. Hu, B. Sanz-Izquierdo, and X. Yang, "Low-profile wideband circularly polarized array antennas using integrated half-power quadrature power divider," *IEEE Trans. Antennas Propag.*, vol. 70, no. 9, pp. 8077–8085, Sep. 2022, doi: 10.1109/TAP.2022.3164885.
[39] Y. Cheng and Y. Dong, "Wideband circularly polarized split patch antenna loaded with suspended rods," *IEEE Antennas Wireless Propag. Lett.*, vol. 20, no. 2, pp. 229–233, Feb. 2021, doi: 10.1109/LAWP.2020.3045988.
[40] M. A. R. Hashmi and P. V. Brennan, "A LHCP printed cross dipole antenna for glacial environmental sensor networks," in *Proc. 52nd Eur. Microw. Conf. (EuMC)*, Milan, Italy, Sep. 2022, pp. 620–623, doi: 10.23919/EuMC54642.2022.9924499.
[41] M. A. Rehman Hashmi and P. V. Brennan, "A low profile wideband RHCP printed Archimedean spiral antenna for glacial telemetry applications," in *Proc. Asia–Pacific Microw. Conf. (APMC)*, Yokohama, Japan, Nov. 2022, pp. 632–634, doi: 10.23919/APMC55665.2022.9999868.
[42] M. A. R. Hashmi and P. V. Brennan, "An improved RHCP Archimedean spiral antenna for glacial environmental sensor networks," in *Proc. Int. Symp. Antennas Propag. (ISAP)*, Sydney, NSW, Australia, Oct. 2022, pp. 395–396, doi: 10.1109/ISAP53582.2022.9998827.
[43] H. T. Friis, "A note on a simple transmission formula," *Proc. IRE*, vol. 34, no. 5, pp. 254–256, May 1946, doi: 10.1109/JRPROC.1946.234568.
[44] J. W. Glen and J. G. Paren, "The electrical properties of snow and ice," *J. Glaciol.*, vol. 15, no. 73, pp. 15–38, 1975, doi: 10.3189/S0022143000034249.
[45] H. Corr, J. C. Moore, and K. W. Nicholls, "Radar absorption due to impurities in Antarctic ice," *Geophys. Res. Lett.*, vol. 20, no. 11, pp. 1071–1074, Jun. 1993, doi: 10.1029/93GL01395.
[46] S. Fujita, T. Matsuoka, T. Ishida, K. Matsuoka, and S. Mae, "A summary of the complex dielectric permittivity of ice in the megahertz range and its applications for radar sounding of polar ice sheets," in *Proc. Int. Symp. Phys. Ice Core Rec.* Hokkaido: Hokkaido Univ. Press, 2000, pp. 185–212. Accessed: Nov. 14, 2022. [Online]. Available: https://eprints.lib.hokudai.ac.jp/dspace/bitstream/2115/32469/1/P185-212.pdf
[47] K. Matsuoka, J. A. MacGregor, and F. Pattyn, "Predicting radar attenuation within the Antarctic ice sheet," *Earth Planet. Sci. Lett.*, vols. 359–360, pp. 173–183, Dec. 2012, doi: 10.1016/J.EPSL.2012.10.018.
[48] Constantine A. Balanis, *Antenna Theory: Analysis and Design*, 4th ed. Hoboken, NJ, USA: Wiley, 2016. Accessed: Dec. 9, 2022. [Online]. Available: https://www.wiley.com/en-gb/Antenna+Theory%3A+Analysis+and+Design%2C+4th+Edition-p-9781118642061
[49] S. Barwick, D. Besson, P. Gorham, and D. Saltzberg, "South polar in situ radio-frequency ice attenuation," *J. Glaciol.*, vol. 51, no. 173, pp. 231–238, 2005, doi: 10.3189/172756505781829467.
[50] J. A. Aguilar, "In situ, broadband measurement of the radio frequency attenuation length at Summit Station, Greenland," *J. Glaciol.*, vol. 68, pp. 1234–1242, May 2022, doi: 10.1017/JOG.2022.40.
[51] S. X. Ta, I. Park, and R. W. Ziolkowski, "Crossed dipole antennas: A review," *IEEE Antennas Propag. Mag.*, vol. 57, no. 5, pp. 107–122, Oct. 2015, doi: 10.1109/MAP.2015.2470680.
[52] I. J. Bahl and D. K. Trivedi, "A designer's guide to microstrip line," *Microwaves*, vol. 16, pp. 174–182, May 1977.
[53] S. Chaudhuri, M. Mishra, R. S. Kshetrimayum, R. K. Sonkar, S. Bhattacharjee, and B. Saha, "High port-to-port isolation dual circularly polarised microstrip patch antenna with multifunction DGS," *IET Microw., Antennas Propag.*, vol. 14, no. 15, pp. 1960–1968, Dec. 2020, doi: 10.1049/IET-MAP.2020.0094.
[54] C. D. S. and S. S. Karthikeyan, "A novel broadband dual circularly polarized microstrip-fed monopole antenna," *IEEE Trans. Antennas Propag.*, vol. 65, no. 3, pp. 1410–1415, Mar. 2017, doi: 10.1109/TAP.2016.2647705.

MUHAMMAD ABDUR REHMAN HASHMI (Graduate Student Member, IEEE) received the bachelor's degree in electronic engineering and the M.S. degree in electrical (communication) engineering from the Pakistan Navy Engineering College (PNEC), National University of Sciences and Technology (NUST), Karachi, in 2007 and 2017, respectively. He is currently pursuing the Ph.D. degree in electronic and electrical engineering with University College London (UCL), U.K. He has over ten years of experience working in the industry. His research interests include RF/microwave antennas and circuit design, environmental sensor networks, underwater acoustics, image processing, and audio signal processing.

PAUL V. BRENNAN was born in London, U.K., in 1963. He received the B.Sc.(Eng.) and Ph.D. degrees in electronic and electrical engineering from University College London (UCL), in 1984 and 1988, respectively.

After a short spell working on agile transceivers with Plessey Military Communications, he joined UCL, as a Research Fellow, where he is currently a Professor of microwave electronics. He is highly active as a Consultant. He is also the Deputy Head of the Electronic and Electrical Engineering Department, UCL, and the Head of the Sensors, Systems and Circuits Research Group. He has published widely in many areas, including radio frequency and microwave electronics, antennas, radar, and phase-locked loops, including a textbook *Phase-Locked Loops: Principles and Practice* (McGraw-Hill/Macmillan, 1996). His current research interests include MIMO/phased array radar imaging systems for geophysical applications, such as snow avalanches and Antarctic ice shelves, radar location systems, phased array and other antenna systems, phase-locked loops, and general RF/microwave electronics.

Prof. Brennan is a member of the Rolls Royce Electrical, Control Systems and Electronics Advisory Board. He is a fellow of the Institute of Engineering and Technology.